ADVANCED MATERIALS
www.advmat.de

Spatiotemporal Design of the Metal–Organic Framework DUT-8(M)

*Hiroki Miura, Volodymyr Bon, Irena Senkovska, Sebastian Ehrling, Nadine Bönisch, Gerrit Mäder, Stefan Grünzner, Azat Khadiev, Dmitri Novikov, Kartik Maity, Andreas Richter, and Stefan Kaskel**

Switchable metal–organic frameworks (MOFs) change their structure in time and selectively open their pores adsorbing guest molecules, leading to highly selective separation, pressure amplification, sensing, and actuation applications. The 3D engineering of MOFs has reached a high level of maturity, but spatiotemporal evolution opens a new perspective toward engineering materials in the 4th dimension (time) by *t*-axis design, in essence exploiting the deliberate tuning of activation barriers. This work demonstrates the first example in which an explicit temporal engineering of a switchable MOF (DUT-8, $[M_1M_2(2,6\text{-ndc})_2\text{dabco}]_n$, 2,6-ndc = 2,6-naphthalene dicarboxylate, dabco = 1,4diazabicyclo[2.2.2]octane, M_1 = Ni, M_2 = Co) is presented. The temporal response is deliberately tuned by variations in cobalt content. A spectrum of advanced analytical methods is presented for analyzing the switching kinetics stimulated by vapor adsorption using in situ time-resolved techniques ranging from ensemble adsorption and advanced synchrotron X-ray diffraction experiments to individual crystal analysis. A novel analysis technique based on microscopic observation of individual crystals in a microfluidic channel reveals the lowest limit for adsorption switching reported so far. Differences in the spatiotemporal response of crystal ensembles originate from an induction time that varies statistically and widens characteristically with increasing cobalt content reflecting increasing activation barriers.

1. Introduction

MOFs stand out in terms of specific surface area and modular design.[1] They find emerging applications in CO_2 capture,[2] water harvesting,[3] gas separation,[4] sensing,[5] and environmental applications.[6] Their industrialization has been propelled recently by SMEs and larger companies, and scalability has been demonstrated.[2a]

A unique feature of some MOFs is their ability to adapt their pore size as a response to a chemical stimulus and open and close their pores reversibly, a phenomenon termed "switchability," or "softness," or more generally addressed as "flexibility."[7] Switchability implies a step-wise specific response (solid-state phase transition) at a well-defined chemical potential (or gas pressure) in contrast to irregular polymers that more often tend to absorb gases gradually and swell continuously. It is exactly this repeatable and step-wise switching behavior which leads to outstanding performance in gas storage,[8] separation,[9] mechanical energy storage,[10] sensing, and molecular recognition effects.[11]

Among the early MOFs recognized to show switchability is ELM-11 (ELM = elastic layered metal–organic framework), a pillared-layer structure showing prototypical gating behavior,[12] while MIL-53 (MIL = Matérial de l'Institut Lavoisier) was the first breathing structure.[13] A key feature of such frameworks is bistability,

H. Miura, V. Bon, I. Senkovska, N. Bönisch, K. Maity, S. Kaskel
Inorganic Chemistry I
Technische Universität Dresden
Bergstrasse 66, 01062 Dresden, Germany
E-mail: stefan.kaskel@tu-dresden.de
H. Miura
Nippon Steel Corporation
20-1 Shintomi, Futtsu, Chiba 293-8511, Japan
The ORCID identification number(s) for the author(s) of this article can be found under https://doi.org/10.1002/adma.202207741.

DOI: 10.1002/adma.202207741

S. Ehrling
3P INSTRUMENTS GmbH & Co. KG
Branch office Leipzig
Bitterfelder Str. 1-5, 04129 Leipzig, Germany
G. Mäder, S. Kaskel
Fraunhofer Institute of Materials and Beam Technology
Wintergerbstr. 28, 01277 Dresden, Germany
S. Grünzner, A. Richter
Professur Mikrosystemtechnik
Technische Universität Dresden
01062 Dresden, Germany
A. Khadiev, D. Novikov
P23 group
Petra III Synchrotron
DESY
Notkestraße 85, 22607 Hamburg, Germany

that is, contracted and open pore phases (cp, op) represent local or global minima on a free energy surface.[14] Gating and breathing can be distinguished as a response of cp or op phase, respectively, representing the global minimum in the absence of guests.[15]

While numerous studies have addressed the function of switchable MOFs under quasi-equilibrium conditions, only a few studies have addressed their dynamic response and spatiotemporal evolution experimentally.[16] The energetic landscape and transition paths characterizing the switching process of dynamic MOFs, are virtually unexplored.

Activation barriers, controlling the recognition of molecules and their transformation, play a crucial role in the physics of life, catalysis, recognition, etc.[11] The deliberate design of activation barriers controlling the spatiotemporal evolution of MOFs will elevate responsive frameworks to a higher level of exploration. The implications for applications in gas separation, sensing, bio-interfaces, and information encoding have been highlighted recently.[15c,17] The ability of switchable MOFs to simultaneously detect and abate toxic vapors combined with a temporal actuation response is a unique feature. Functional frameworks with a more complex energetic landscape involving hydrogen bonding interactions show selective molecular recognition effects.[11] However, kinetic recognition coupled to structural reorganization, a key feature of enzyme key-lock interactions, and the corresponding understanding of the spatiotemporal evolution of frameworks is in its infancy. Main challenges arise from the theoretical side to include real time axis in simulations covering finite size effects of relevant crystal dimensions. Schmid et al. have simulated the spatiotemporal evolution of dynamic nanocrystals under external pressure.[18] Speybroeck et al.[19] have proposed phase coexistence in MIL-53 and Co(1,4-benzenedipyrazolate) (CoBDP)[8,20] to play an important role in the transformation mechanism and have analyzed the size-dependent grain boundary formation in individual crystals.

Energetic barriers controlling kinetics may not only arise from the framework bistability but are coupled to the physics of the guest molecules with characteristic barriers of fluid nucleation, diffusion, and adsorption processes. So far, an accurate assessment of switchable MOF transformation time has not been achieved. The pioneering work by Tanaka et al. has assessed for the first time the transformation kinetics of ELM-11 via time-resolved synchrotron X-ray diffraction studies revealing macroscopic timescales of the order of seconds.[16a]

However, these measurements represent an ensemble of crystals and give only limited insights into individual crystal transformation rates. Moreover, the kinetics of ELM-11 can only be varied by adjusting the externally controlled variables such as guest activity and temperature. Li and co-workers investigated the rate of adsorption coupled with the structural transition in a flexible MOF (RPM3_Zn) by pressure drop experiments.[21] Kitagawa and co-workers recently reported on the direct observation of the guest response of the surface on a single-crystalline pillared-layer MOF, by in situ liquid-phase AFM upon biphenyl adsorption.[22]

Our vision is to tune the spatiotemporal response of metal–organic frameworks by synthesis and design and to engineer materials along a time-axis[17] (*t*-axis design). In the following, we demonstrate for the first time experimentally the deliberate tuning of activation barriers in a switchable, gate pressure MOF model system DUT-8(M) (DUT = Dresden University of Technology, M = Ni/Co) leading to a temporally controlled response. The stiffness of the metal node is used to deliberately tune the gate opening rate. We analyze the different ensemble switching rates by physisorption methods, advanced in situ synchrotron XRD analysis and for the first time provide an insight into individual crystal response rates using a new microfluidic breakthrough-apparatus that allows us to optically record the spatiotemporal evolution in situ under a dynamic gas flow.

2. Results and Discussion

DUT-8(Ni) is a gating MOF that stands out in terms of huge volume expansion upon exposure to fluids such as N_2 (77 K), CO_2 (196 K, 298 K), CH_2Cl_2 (298 K), *n*-butane (298 K), Ar (87 K), or Xe (165 K).[23] High selectivity of DUT-8(Ni) for CO_2/CH_4 separation has been reported to rely on the almost exclusive adsorption of CO_2 in the presence of methane as analyzed by in situ NMR spectroscopy.[24] The framework is assembled from paddle wheels and 2,6-naphthalene dicarboxlyate linkers to form 4,4-nets, which are stacked perpendicular to the layer by coordination of dabco (1,4-diazabicyclo[2.2.2]octane) on the axial coordination site of the paddle wheel (**Figure 1**a). The framework is variable in composition and the substitution of various metals (M = Co, Ni, Zn, Cu) has been reported elsewhere.[23a,b,d,25] In particular, the partial substitution of Ni by Co leads to mixed metal frameworks showing a systematic variation in the gate-opening pressure (Figure 1b).[26] Theoretical studies proposed the gate opening pressure to be controlled by the activation barrier while the gate closing pressure is closer to the expected equilibrium pressure of the phase transition.[27] The unsubstituted DUT-8(Ni) undergoes a structural opening transition at an average relative adsorption pressure of $p_{APHM}/p_0 = 0.12$ for N_2 (77 K) and 0.20 for dichloromethane (DCM, 298 K) (p_{APHM} = adsorption pressure at half maximum,[28] Figure 1b,c; Figure S3, Table S1, Supporting Information). With increasing cobalt content, p_{APHM}/p_0 reaches 0.40 for N_2 at 50% substitution and higher Co content leads to an incomplete opening of the ensemble. For DCM the APHM varies more gradually and even pure DUT-8(Co) responds well with about 68% uptake compared to DUT-8(Ni) (Figure 1b,c; Figure S3, Table S1, Supporting Information). These features demonstrate efficient tailoring of the gate opening pressure under quasi-equilibrium conditions. The branches for DCM desorption superimpose (Figure 1c), indicating that the closing upon desorption occurs in equilibrium while the opening process is the critical switching step, kinetically controlled by a tunable activation barrier.

Others and we have hypothesized that this gate opening pressure reflects an activation barrier and directly translates into the macroscopic and microscopic temporal evolution of MOF crystals.[16a,17] To gain deeper insights into the interplay of gate opening pressure and the phase transformation rate, we first analyzed macroscopic crystal ensembles. The framework powders were subjected to a defined DCM vapor pressure and the pressure drop was monitored to analyze the adsorption kinetics.

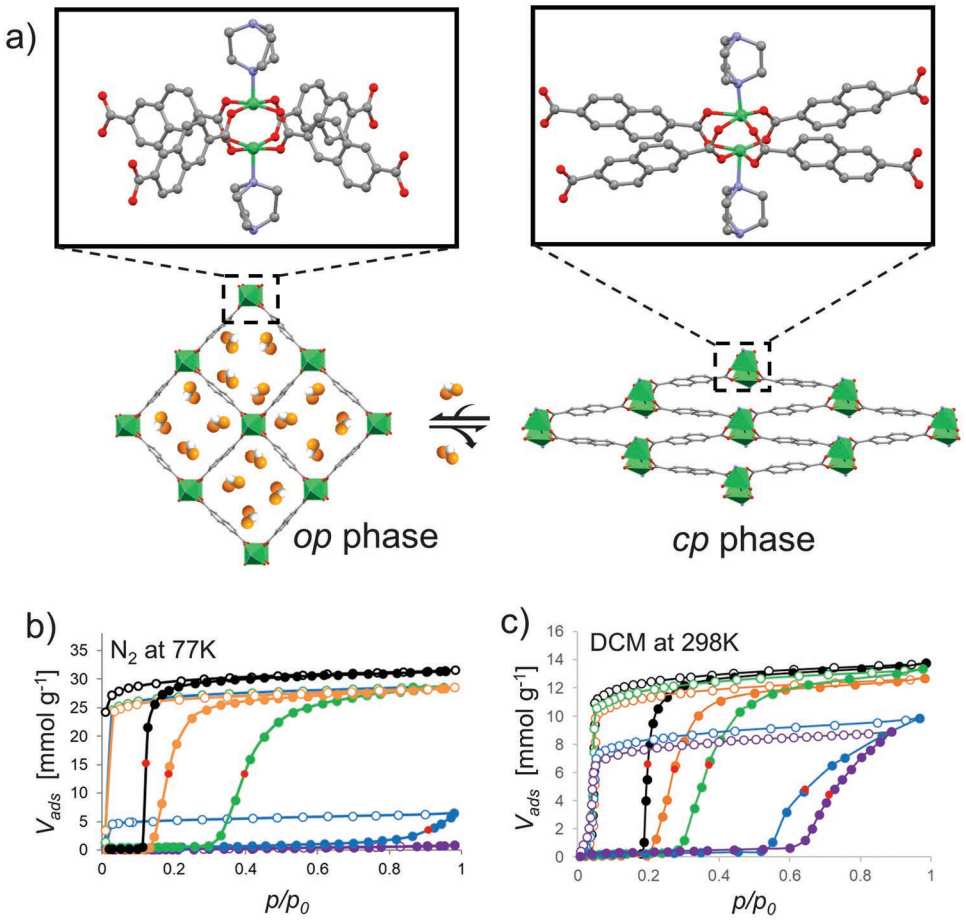

Figure 1. a) Structural transition of DUT-8(Ni) between op and cp phases. Nickel—in green, carbon—in gray, oxygen in red, nitrogen—in blue, chlorine in orange, and hydrogen—in yellow. The hydrogen atoms of the framework are omitted for clarity. b) N_2 physisorption isotherms at 77 K and c) DCM physisorption isotherm at 298 K on DUT-8(Ni) (black) DUT-8($Ni_{0.75}Co_{0.25}$) (orange), DUT-8($Ni_{0.50}Co_{0.50}$) (green), DUT-8($Ni_{0.25}Co_{0.75}$) (blue), and DUT-8(Co) (purple). The adsorption branch is represented by solid symbols and the desorption branch—by empty symbols. A red circle indicates APHM.

The cell with about 10 mg of DUT-8(Ni)_cp, connected to the volumetric instrument, was evacuated and the dosing pressure ($p_{Ini,\ Mani}$) in the manifold was set to 95 kPa. After the introduction of DCM vapor, the pressure in the sample cell increased quickly to 57.4 kPa (p_{Max}) at 298 K and further gradually decreased due to the adsorption. Then the pressure was equilibrated to reach 50.4 kPa (p_{Fin}) after 100 s. As a reference, the pressure drop in the empty cell, as well as in the cell containing a rigid version of DUT-8(Ni)[29] were measured (Figure S17, Supporting Information), showing the slowest kinetic for the flexible DUT-8(Ni) sample.

We also investigated the adsorption rate of DUT-8(Ni) with different dosing pressures of 85, 75, 65, and 55 kPa at 298 K (**Figure 2**a). By decreasing dosing DCM pressure, the adsorption rate became evidently slower. In this experiment, the overpressure Δp ($\Delta p = p_{max} - p_{APHM}$) plays the essential role driving the nucleation of phase transition, similar to the undercooling (ΔT) for temperature-driven transitions or supersaturation in precipitation reactions.[30] The pressure profile data were analyzed based on the Kolmogorov–Johnson–Mehl–Avrami (KJMA) Equation (1).[31]

$$a = 1 - \exp\left(-kt^n\right) \quad (1)$$

where a is the fraction of pressure drop at time t, k is the rate constant, and n is the dimension of the phase transition (the Avrami exponent). For a channel-like porosity of DUT-8, the n is expected to be close to 1. For better comparison of the rate constants, the pressure drop curves were fitted to Equation (1), where n was fixed to 0.93. The obtained parameters are summarized in **Table 1**.

The k values were estimated as 0.034, 0.030, 0.027, 0.023, and 0.019 at 95, 85, 75, 65, and 55 kPa of dosing pressure, respectively. A linear relationship is characteristic for the correlation of rate constant k and the pressure difference, $p - p_{APHM}$,[16a] where p is the DCM pressure introduced into the sample cell with DUT-8(Ni) and p_{APHM} is the gate-opening pressure.

Our main target is to demonstrate the deliberate tuning of the activation barriers and its implications for the temporal response rate by chemical design. Hence, we investigated the impact of cobalt doping in DUT-8($Ni_{1-x}Co_x$) on the adsorption rate in the pressure drop experiment (**Figure 3**). The typical half-time for a 50% pressure drop was 25, 27, 46, 54, and 89 s for 0%, 25%, 50%, 75%, and 100% Co content, respectively, confirming a direct relation of p_{APHM} and the adsorption kinetics. The pressure drop kinetics follow the KJMA equation

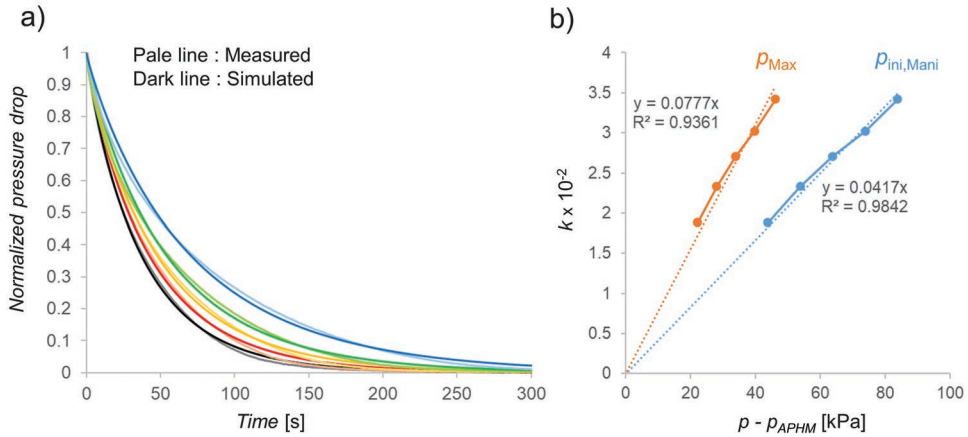

Figure 2. a) Normalized pressure drop curves obtained at different dosing pressures ($p_{ini,Mani}$): 95 kPa in black, 85 kPa in red, 75 kPa in orange, 65 kPa in green, and 55 kPa in blue; b) Relationship between the rate constants and the pressure difference between the initial DCM vapor pressure p, and the gate opening pressure p_{APHM} (when p_{Max} or $p_{ini,Mani}$ were used as p the points shown in orange or blue were obtained, respectively).

(Equation (1)) and the rate constants k are summarized in **Table 2**. A monotonic dependence of k on p–p_{APHM} was found but a discontinuity is observed between 50% and 75% Co for the samples that did not achieve the full expected uptake. This nonlinear relationship indicates a critical cobalt concentration at which the clustering of Co_2-paddle wheels leads to a pronounced deviation from a purely statistical distribution of Co^{2+} and Ni^{2+} ions. This finding is also supported by EPR studies.[26]

The rate of DCM adsorption was also investigated in breakthrough experiments at 302 K (Figure S12, Supporting Information). The structural transition of DUT-8(Co) does not take place under the conditions of the experiment; therefore, this measurement can be seen as a reference for an immediate breakthrough. The dynamic experiments confirm the results of the pressure drop experiments, showing that DUT-8(Ni) responds and reaches the full uptake much faster compared to the cobalt-containing frameworks.

As the adsorption kinetics indicate a rather slow switching (50–300 s) of the MOF materials, we were curious if the structural opening transformation could be observed on the same time scale. In situ PXRD investigations were carried out at the DESY synchrotron (Hamburg) to directly observe the pore opening with a high time resolution after imposing a pressure pulse on the crystal ensemble (**Figure 4**; Figure S19, Supporting Information). The phase transition is clearly detected after a few seconds (DUT-8(Ni)) by the rise of the (110) peak at 0.49 $Å^{-1}$ of the DUT-8(Ni)_op phase. The peak intensities of the op phase were analyzed on the basis of the KJMA equation (where α is the fraction of op phase at time t) but the index n varied for the different samples, which made it difficult to compare the k parameters directly (**Table 3**).

As expected, DUT-8(Ni) shows the fastest phase transformation while the Co substituted samples are much slower. The in situ time-resolved PXRD data are in good agreement with the adsorption rate experiments. However, it is interesting to see that the structural transformation rates are generally much faster than the rates derived from volumetric adsorption data. One of the reasons for that could be the difference in the $\Delta p = p_{max}$–p_{APHM} in the two different experimental setups since the amount of sample used is an order of magnitude less than the sample amount used in the pressure drop experiments at comparable dead volume of the system. Another aspect is the differences in mass transport constants in the two systems.

2.1. Individual Crystal Analysis

A key open question not addressed in any previous work is: What is the actual transformation rate of individual switchable MOF crystals? Do individual crystals require several ten seconds to open?

To shine a light on these questions, we designed a novel microfluidic breakthrough apparatus adapted to a gas-dosing unit and a high-quality optical microscope (**Scheme 1**). The

Table 1. Summary of experimental and calculated parameters for DCM pressure drop profile analysis on DUT-8(Ni) applying different dosing pressure at 298 K (p_0 = 56.9 kPa).

Sample	Weight [mg]	k [×10^{-2}]	R^2	$p_{ini,Mani}$ [kPa]	p_{max} [kPa]	p_{fin} [kPa]	Δp [kPa]
DUT-8(Ni)[a]	10.3	3.420	0.9991	95.0	57.4	50.4	46.2
	10.4	3.016	0.9987	85.0	50.9	44.0	39.7
	10.1	2.707	0.9986	75.0	45.1	37.6	33.9
	10.0	2.331	0.9981	65.0	38.4	31.7	27.2
	10.1	1.883	0.9969	55.0	33.3	26.0	22.1

[a]p_{APHM} for the sample is 11.2 kPa (p/p_0 = 0.20).

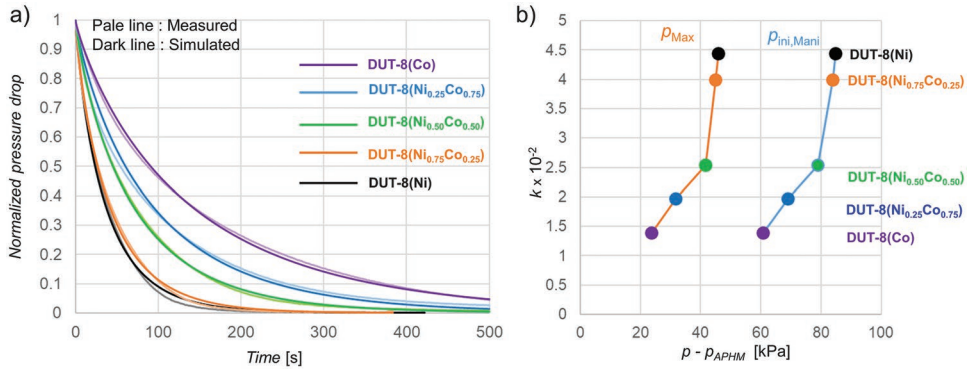

Figure 3. a) Normalized DCM pressure drop curves obtained for DUT-8(Ni) (black) DUT-8($Ni_{0.75}Co_{0.25}$) (orange), DUT-8($Ni_{0.50}Co_{0.50}$) (green), DUT-8($Ni_{0.25}Co_{0.75}$) (blue), and DUT-8(Co) (purple) at 298 K; b) Relationship between the rate constants and the pressure difference between the DCM vapor pressure and APHM.

chamber for sample observation is 0.5 × 0.5 mm in cross section and 40 mm long and consists of a polydimethylsiloxane channel closed by a glass slide on which the crystals are placed (Figures S10,S11, Supporting Information). The DCM vapor is fed from a saturator operated with mass flow controllers to adjust the total flow to 10 mL min^{-1} and a saturation pressure of 56.9 kPa. To achieve a rapid switch from N_2 to DCM vapor, a three-way valve with minimized dead volume is used. Computational fluid dynamics (CFD) simulations demonstrate that the concentration change in the channel is achieved within 100 ms (Section S7, Supporting Information). This setup allows an individual observation of crystals and their switching rate. Placing crystals differing in composition in the same channel allows a direct comparison of switching rates (Figure S20, Video S1, Supporting Information). For a statistical evaluation of individual crystals, we placed several crystals of the same batch into a channel and analyzed the transformation process. The structural expansion is recognized from the volume change, shape change, and partially also from the color change (Figure S21, Supporting Information).

Initially, the structural transition of DUT-8(Ni) crystals was observed directly through microscopy by using different concentrations of DCM vapor (simulating different $\Delta p = p_{max} - p_{APHM}$). The dosing DCM vapor was diluted to 80%, 70%, 60%, and 50% by mixing with pure N_2 gas (Videos S2–S5, Supporting Information).

This novel technique reveals important new findings evident from the videos and their statistical analysis: The individual transformation time for a single crystal is only 3–4 frames (camera 9 fps) and, in some cases, only one frame. Hence, the actual timescale of transformation for an individual crystal is typically below 1 s. This observation is quite astonishing and not accessible from bulk analysis techniques that reveal much slower switching processes, as discussed above. In some cases, a beginning transformation can be discerned on one end of the crystal and the transition front propagates rapidly through the crystal. This is even true for crystals that are broken into smaller fractions before the gas is introduced. The propagation wave moves rapidly over the fracture (Video S6, Supporting Information).

Despite the fact, that the switching of individual crystals proceeds with apparently the same, very fast rate for all crystals, the crystals do not switch all at the same time after introducing the vapor. A significant delay is observed after the vapor reaches the cell and some crystals switch earlier and some later with a characteristic statistical distribution. In the following, this time delay is termed induction time.

By using the time (t_1) of the first switching crystal as an indicator that the gas has filled the channel, we can directly compare the induction time for the following crystals (t_n) by defining the normalized switching time $\hat{t}_n$:

$$\hat{t}_n = t_n - t_1 \tag{2}$$

Decreasing the concentration of DCM vapor from 100% to 60%, the distribution of normalized induction times broadens. For 50% DCM vapor the distribution appears narrower than that for 70% and 60% DCM vapor (**Figure 5**), however, the number of crystals remaining as cp phase increased for such low DCM concentrations (Figure S25, Supporting Information).

In order to demonstrate the engineering of the framework's temporal response by chemical design, DUT-8(Ni),

Table 2. Summary of experimental and calculated parameters for DCM pressure drop profile analysis on DUT-8(Ni), DUT-8($Ni_{0.75}Co_{0.25}$), DUT-8($Ni_{0.50}Co_{0.50}$), DUT-8($Ni_{0.25}Co_{0.75}$), and DUT-8(Co) at 298 K (p_0 = 56.9 kPa). Avrami exponent n = 0.87.

Sample	Weight [mg]	k [$\times 10^{-2}$]	$R2$	$p_{ini,Mani}$ [kPa]	p_{max} [kPa]	p_{fin} [kPa]	p_{APHM} [kPa]
DUT-8(Ni)	10.6	4.434	0.9972	95.1	56.1	50.0	11.4
$Ni_{0.75}Co_{0.25}$	10.5	3.996	0.9979	94.9	55.9	49.4	15.6
$Ni_{0.50}Co_{0.50}$	10.4	2.538	0.9993	95.0	57.8	51.0	21.2
$Ni_{0.25}Co_{0.75}$	10.3	1.973	0.9942	94.9	57.6	50.3	37.1
DUT-8(Co)	10.4	1.383	0.9988	95.0	57.8	51.0	40.8

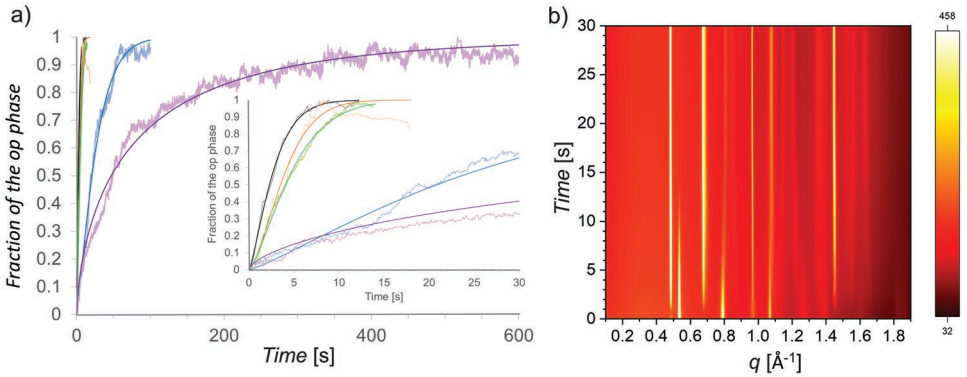

Figure 4. a) Fractions of the open pore phase for DUT-8(Ni) (black), DUT-8($Ni_{0.75}Co_{0.25}$) (orange), DUT-8($Ni_{0.50}Co_{0.50}$) (green), DUT-8($Ni_{0.25}Co_{0.75}$) (blue), and DUT-8(Co) (purple) at room temperature based on in situ synchrotron PXRD measurements. Each pale color jagged symbols correspond to the change in the normalized peaks intensity and the lines with dark color were obtained by fitting the experimental data to the KJMA equation; b) Color map of in situ PXRD patterns collected upon DCM adsorption on DUT-8(Ni) at 298 K.

DUT-8($Ni_{0.75}Co_{0.25}$), DUT-8($Ni_{0.50}Co_{0.50}$), DUT-8($Ni_{0.25}Co_{0.75}$), and DUT-8(Co) crystals were directly analyzed through microscope by dosing DCM vapor. In the case of DUT-8(Ni) and DUT-8($Ni_{0.75}Co_{0.25}$) crystals, all of the crystals showed the start of structural transition within a few seconds. On the other hand, few crystals showed the start of structural transition only after 2.5 h. Statistical analysis is provided in **Figure 6**: For pure DUT-8(Ni) the induction time is below 2 s for all crystals. A similar observation is made for DUT-8($Ni_{0.75}Co_{0.25}$), but a few crystals have a longer induction time of up to 9 s. For 50% Co substitution this tendency is pronounced: While the majority of crystals switches after a few seconds, a considerable amount of crystals has induction periods of 5–20 s. Moreover, 15% of DUT-8($Ni_{0.50}Co_{0.50}$) crystals remained in the cp phase (Figure S24, Supporting Information). Most of DUT-8($Ni_{0.25}Co_{0.75}$) and DUT-8(Co) crystals remained in the contracted pore phase which is in accordance with the reduced total uptake observed in the DCM isotherms (Figure 1c).

These observations are important as they give unprecedented insights into the real spatiotemporal evolution of individual MOF crystals.

1) The individual transformation rate is extremely fast and can reach fractions of seconds. The differences in the individual transformation rate are insignificant compared to the temporal resolution of the instruments used. Individual transformations are orders of magnitude faster than the transformation time measured for an ensemble (10–300 s).

Table 3. Summary of experimental and calculated parameters for in situ synchrotron PXRD measurements on DUT-8(Ni), DUT-8($Ni_{0.75}Co_{0.25}$), DUT-8($Ni_{0.50}Co_{0.50}$), DUT-8($Ni_{0.25}Co_{0.75}$), and DUT-8(Co) at 298 K.

Sample	*n*	*k*	*R*2	$p_{ini,Mani}$ [kPa]	p_{max} [kPa][a)]
DUT-8(Ni)	1.31	0.238	0.9995	97	46
$Ni_{0.75}Co_{0.25}$	1.51	0.104	0.9919	97	46
$Ni_{0.50}Co_{0.50}$	1.36	0.103	0.9992	97	52
$Ni_{0.25}Co_{0.75}$	1.20	0.018	0.9983	97	52
DUT-8(Co)	0.64	0.05	0.9988	97	50

[a)]In the in situ experiment p_{Max} approximately represents also p_{Fin}, since the amount of the sample in the capillary is small (≈1 mg) and the pressure drop due to the adsorption in the system is not measured. Time resolution is 0.1 fps in all cases.

2) Samples differing in ensemble transformation rate (based on X-ray and volumetric adsorption data) show pronounced differences regarding the individual induction time. With higher gate opening pressure (p_{APHM}) measured in the isotherm of an ensemble, the distribution of individual induction times (induction time variation) broadens significantly and individual crystals switch only after 17 s (DUT-8($Ni_{0.50}Co_{0.50}$)) while some crystals remain closed.

Volumetric pressure drop data show an order of magnitude slower rates for DUT-8($Ni_{0.50}Co_{0.50}$) and the material is not entirely transformed even after 200 s. This discrepancy between uptake rate and individual switching rates indicates that mass transport phenomena in the large cell volume of a volumetric instrument are superimposed on the actual transformation rate of individual crystals. Synchrotron studies reveal a much faster and direct analysis of the transformation rate, indicating an almost complete transformation of DUT-8(Ni) after 15–20 s. However, even in the small volume of the synchrotron capillary, after applying a pressure jump, diffusion limitation in the capillary may be superimposed on the actual crystal transition rates. Only the microscopic analysis discloses the fastest response time accessible so far, providing a lower limit for the individual transformation rate of crystals (below 1 s) and giving for the first time insights into delay phenomena revealing characteristic induction periods for the switching of individual crystals.

Frameworks differing in gate opening pressure are distinguished by characteristic induction time distribution differing in width. This width in induction time is directly related to p_{APHM} and strongly affected by a "smearing" of the adsorption branch (gate opening pressure distribution), a transition from a very steep uptake to a more broadened uptake.[28] The broadened distribution of induction time reflects the transition barrier of individual crystals as the underlying reason for differences in macroscopic ensembles. The same is true if p_{APHM} is constant (DUT-8(Ni)) and the activity of the stimulus (p_{DCM}) is varied. With decreasing $\Delta p = p_{DCM} - p_{APHM,}$ the induction time distribution is widened and a larger number of individual crystals remain closed.

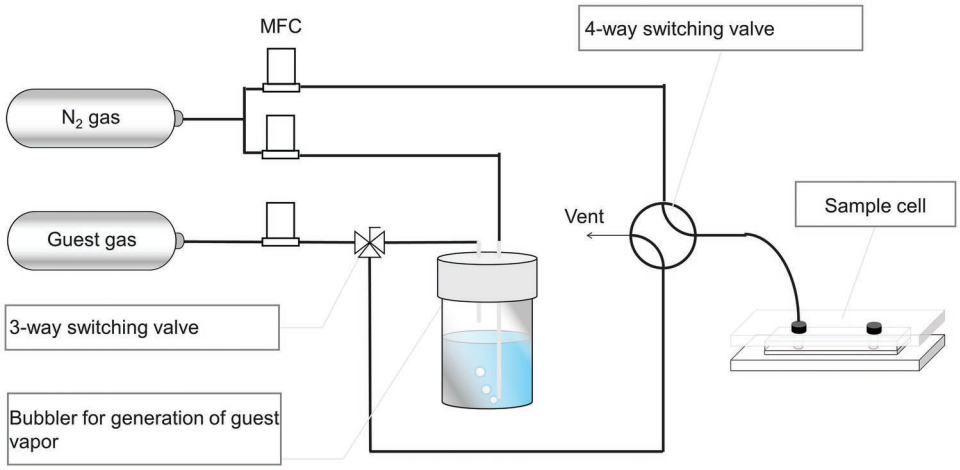

Scheme 1. Schematic drawing of microfluidic breakthrough apparatus.

3. Conclusion

Engineering materials along a time axis represents a new paradigm in materials science. Such frameworks may be also termed 4D materials, as not only their spatial arrangement of atoms is precisely controlled but also their temporal response. Switchable Metal-Organic Frameworks are tailorable along a time axis by chemical design. Their spatiotemporal response is governed by an activation barrier, reflected in the gate opening pressure (p_{APHM}) and the activity of the pore opening stimulating guest molecule (p_{stim}). The ensemble-based switching rate constant k increases with $\Delta p = p_{stim} - p_{APHM}$. Individual crystal transformation rates are orders of magnitude faster than rates estimated based on ensemble methods. However, slow-transforming ensembles show a delayed induction of individual crystal transformations. Ensembles differing in gate opening pressure exhibit significant differences in the distribution of induction times and a wider distribution is characteristic for decreasing Δp.

Engineering 4D materials is equivalent to a deliberate control of activation barriers in materials science, a hitherto rarely explored scientific field. In nature, the recognition of molecules is controlled by kinetic barriers regulating catalytic activity, key-lock interactions and the response of enzymes. We expect the

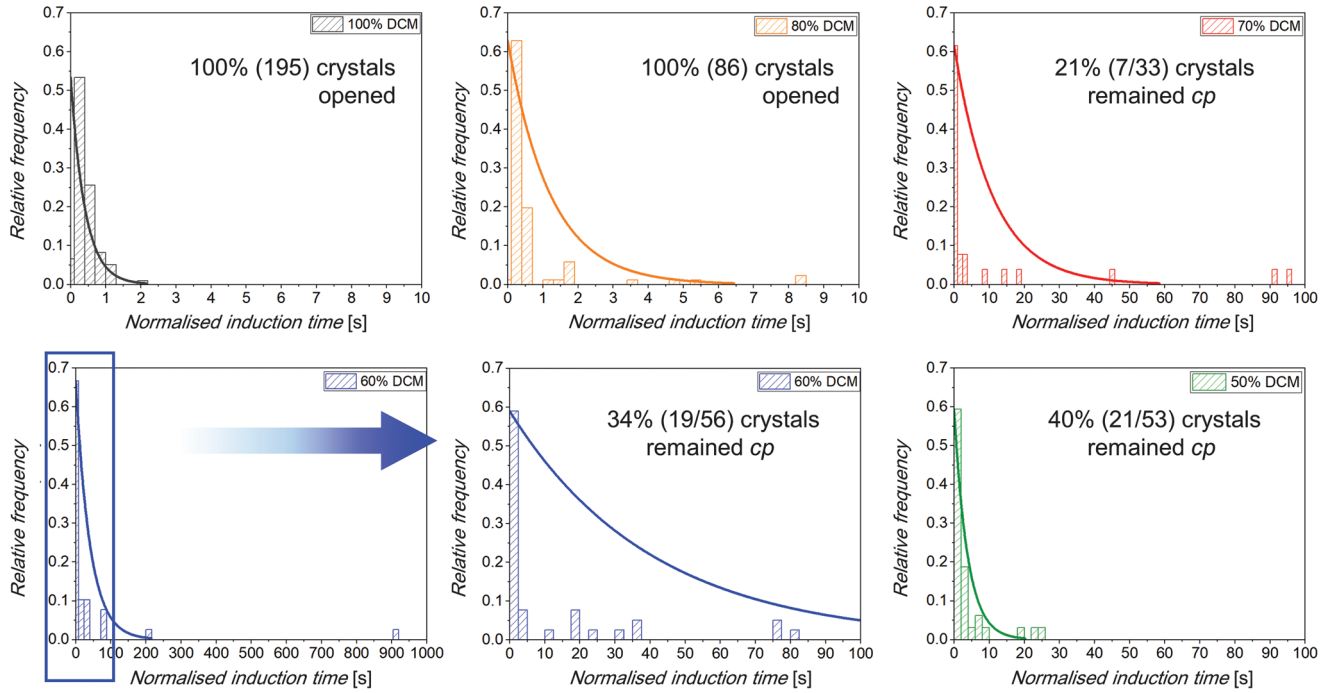

Figure 5. a) Normalized induction time histograms for different DCM vapor concentrations investigated (black = 100%, orange = 80%, red = 70%, blue = 60%, and green = 50%) for DUT-8(Ni) fitted by an exponential density probability function. The λ value (the mean number of events in an interval of time) is 2.46 for 100%, 0.82 for 80%, 0.09 for 70%, 0.025 for 60%, 0.26 for 50%.

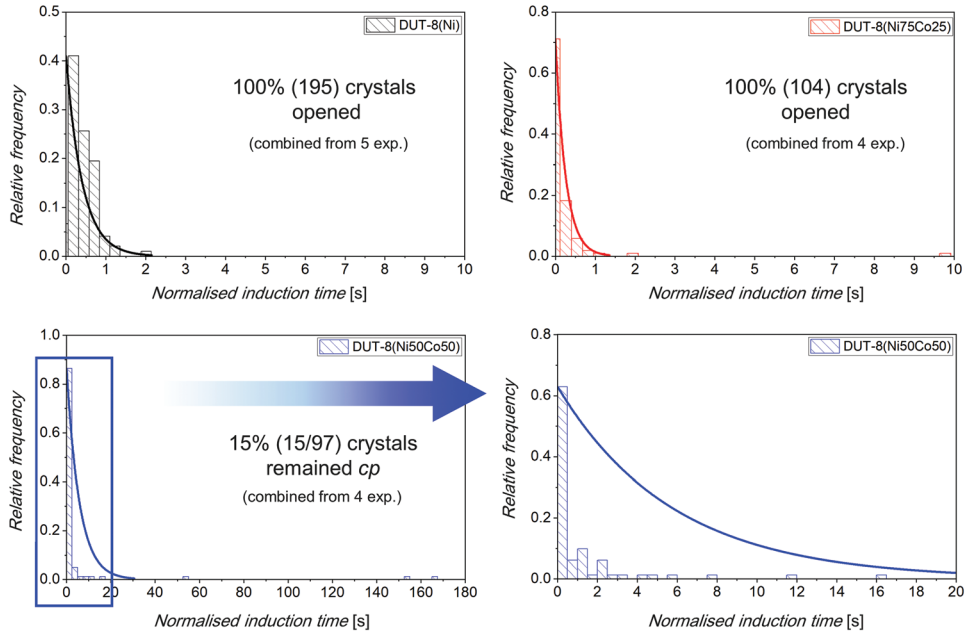

Figure 6. Normalized induction time histograms of DUT-8(Ni) (black), DUT-8($Ni_{0.75}Co_{0.25}$) (red), and DUT-8($Ni_{0.50}Co_{0.50}$) (blue) crystals fitted by an exponential density probability function (The λ value is 2.46 for DUT-8(Ni), 3.89 for DUT-8($Ni_{0.75}Co_{0.25}$), and 0.17 for DUT-8($Ni_{0.50}Co_{0.50}$)).

deliberate control of activation barriers in dynamic frameworks to play a decisive role in selective recognition in molecular separation, catalysis, sensing, and actuation. A *t*-axis design will enable the production of actuators with controlled response time performing fast or slow dynamic movements depending on requirements. For predictive simulations, nucleation and propagation of phonons through a MOF crystal are essential phenomena to be addressed in the future. Patterning and positioning of dynamic materials in devices may create more complex machines with time-controlled active hinges, artificial pumps, or microfluidic valves. In the future, we expect frameworks to perform more complex motions such as periodic oscillations, acceleration, damping, or folding transformations. The installation of an "internal clock" controlling the spatiotemporal design of individual crystals is a long-term vision. Advanced time resolved methods and control over microstructure, defects and crystal interfaces will be decisive in achieving a deep understanding of individual crystal transformation rates in the future.

4. Experimental Section

Synthesis: The materials were synthesized according to the slightly modified synthetic procedures reported in ref. [26]. For more details see Section S1, Supporting Information. The phase purity of the compounds was verified by powder X-ray diffraction (Figure S1, Supporting Information). The samples were washed with *N,N*-dimethylformamide several times and afterward, the samples were washed with DCM several times by decantation. The resulting solids were filtered in an argon flow and desolvated applying dynamic vacuum at room temperature overnight to form the closed pore phases (Figure S2, Supporting Information).

Physisorption Isotherms: Volumetric low-pressure nitrogen and DCM physisorption isotherms were measured on a BEL-Max instrument (Microtrac MRB). Helium gas of 99.999% purity was used for the determination of the dead volume and nitrogen gas of 99.999% purity was used as adsorptive. DCM with a purity of 99.9% was used for vapor adsorption experiment. The samples were degassed at 393 K in dynamic vacuum for at least 6 h before the measurement.

Pressure Drop DCM Adsorption Experiments: The experiments were performed on a BEL-Max instrument (Microtrac MRB). The sample cell was shortened to reduce the dead volume. The DCM-containing vessel was held at 313 K and the sample cell was set at the respective temperature of interest using a Julabo circulation thermostat. The dosing of the vapor to the sample cell was performed in manual mode. The time interval between the data points was 1 s.

Time-Resolved In Situ PXRD Experiments: Time-resolved in situ PXRD experiments were conducted at P23 in situ diffraction and imaging beamline of PETRA III synchrotron (DESY). Monochromated irradiation with E = 20.0 keV (λ = 0.619921 Å) was used in all experiments. Reflection intensities were measured using PILATUS 1 M (DECTRIS) detector. The distance between the sample and the detector was 45 cm. In a typical experiment, PXRD patterns were collected at a 10 Hz rate during the 300–3600 s. The experimental setup consisted of a volumetric adsorption instrument BELSORP-max (Microtrac MRB), used as a gas handling system, which was connected to the customized home-built in situ glass capillary serving as an adsorption cell (for more details see Section S9, Supporting Information).

Microscopy Experimental Setup: Samples containing DCM in the pores were filtered under Ar flow and desolvated under vacuum at room temperature using Schlenk technique. Subsequently, desolvated samples were transferred to a glovebox. The individual crystals were selected using an optical microscope and transferred into the channel of the microfluidic cell made from PDMS (Figure S10, Supporting Information). The cell was transferred under argon and connected to a dosing system, which allowed to switch between the nitrogen gas flow and the DCM vapor (Scheme 1; Figure S11, Supporting Information). An Olympus GX53 microscope and a camera with frame rates of 9 fps were used for monitoring the switching process. Recording of crystal transition and the statistical analysis were performed using OLYMPUS Stream Essentials 2.4.3 software.

Statistical Analysis: The pressure drop curves and the fraction of the op phase calculated from the in situ PXRD patterns were normalized as follows:

$$y_{\text{normalized}} = \frac{y - y_{\max}}{y_{\max} - y_{\min}} \quad (3)$$

In the microscopy experiments, the time of the first switching event (t_1) was set to zero. The induction time for all the following crystals (t_n) was the normalized switching time $\hat{t}_n$ defined as:

$$\hat{t}_n = t_n - t_1 \tag{4}$$

The relative frequency in the induction time histograms (Figures 5 and 6) was the frequency in a particular class divided by the total number of observations. The total number of observations was given in each graph. The exponential density probability function used for data fitting by OriginPro 2021b software was:

$$y = f(x \mid \lambda) = \lambda e^{-x\lambda} \tag{5}$$

The mean parameter, standard deviation parameter, or scale parameter for the exponential density probability function were:

$$\mu = \frac{1}{\lambda} \tag{6}$$

The λ values for each analysis are given in the figure captions.

Supporting Information

Supporting Information is available from the Wiley Online Library or from the author.

Acknowledgements

The support by DFG (FOR2433) is gratefully acknowledged. The authors acknowledge DESY (Hamburg, Germany), a member of the Helmholtz Association HGF, for the provision of experimental facilities. Parts of this research were carried out at P23 beamline of PETRA III synchrotron. Beamtime was allocated for proposal I-20211060. V.B. acknowledges BMBF Project No 05K19OD2.

Open access funding enabled and organized by Projekt DEAL.

Conflict of Interest

The authors declare no conflict of interest.

Data Availability Statement

The data that support the findings of this study are available in the supplementary material of this article.

Keywords

metal–organic frameworks, nucleation, porous materials, spatiotemporal engineering, stimuli-responsive materials

Received: August 24, 2022
Revised: October 23, 2022
Published online: December 27, 2022

[1] a) M. J. Kalmutzki, N. Hanikel, O. M. Yaghi, *Sci. Adv.* **2018**, *4*, eaat9180; b) Z. Ji, H. Wang, S. Canossa, S. Wuttke, O. M. Yaghi, *Adv. Funct. Mater.* **2020**, *30*, 2000238; c) I. M. Hönicke, I. Senkovska, V. Bon, I. A. Baburin, N. Bönisch, S. Raschke, J. D. Evans, S. Kaskel, *Angew. Chem., Int. Ed.* **2018**, *57*, 13780.

[2] a) J.-B. Lin, T. T. T. Nguyen, R. Vaidhyanathan, J. Burner, J. M. Taylor, H. Durekova, F. Akhtar, R. K. Mah, O. Ghaffari-Nik, S. Marx, N. Fylstra, S. S. Iremonger, K. W. Dawson, P. Sarkar, P. Hovington, A. Rajendran, T. K. Woo, G. K. H. Shimizu, *Science* **2021**, *374*, 1464; b) M. Ding, R. W. Flaig, H.-L. Jiang, O. M. Yaghi, *Chem. Soc. Rev.* **2019**, *48*, 2783; c) H. Demir, G. O. Aksu, H. C. Gulbalkan, S. Keskin, *Carbon Capture Sci. Technol.* **2022**, *2*, 100026.

[3] a) N. Hanikel, M. S. Prévot, O. M. Yaghi, *Nat. Nanotechnol.* **2020**, *15*, 348; b) N. Hanikel, X. Pei, S. Chheda, H. Lyu, W. Jeong, J. Sauer, L. Gagliardi, O. M. Yaghi, *Science* **2021**, *374*, 454; c) W. Xu, O. M. Yaghi, *ACS Cent. Sci.* **2020**, *6*, 1348; d) G. Yilmaz, F. L. Meng, W. Lu, J. Abed, C. K. N. Peh, M. Gao, E. H. Sargent, G. W. Ho, *Sci. Adv.* **2020**, *6*, eabc8605.

[4] a) D. S. Sholl, R. P. Lively, *Nature* **2016**, *532*, 435; b) B. R. Barnett, M. I. Gonzalez, J. R. Long, *Trends Chem.* **2019**, *1*, 159; c) H. Li, K. Wang, Y. Sun, C. T. Lollar, J. Li, H.-C. Zhou, *Mater. Today* **2018**, *21*, 108; d) Q. Qian, P. A. Asinger, M. J. Lee, G. Han, K. Mizrahi Rodriguez, S. Lin, F. M. Benedetti, A. X. Wu, W. S. Chi, Z. P. Smith, *Chem. Rev.* **2020**, *120*, 8161; e) R.-B. Lin, S. Xiang, W. Zhou, B. Chen, *Chem* **2020**, *6*, 337; f) B. Hosseini Monjezi, K. Kutonova, M. Tsotsalas, S. Henke, A. Knebel, *Angew. Chem., Int. Ed.* **2021**, *60*, 15153.

[5] a) H.-Y. Li, S.-N. Zhao, S.-Q. Zang, J. Li, *Chem. Soc. Rev.* **2020**, *49*, 6364; b) J. F. Olorunyomi, S. T. Geh, R. A. Caruso, C. M. Doherty, *Mater. Horiz.* **2021**, *8*, 2387; c) W.-T. Koo, J.-S. Jang, I.-D. Kim, *Chem* **2019**, *5*, 1938; d) L.-T. Zhang, Y. Zhou, S.-T. Han, *Angew. Chem., Int. Ed.* **2021**, *60*, 15192.

[6] a) H. B. Wu, X. W. Lou, *Sci. Adv.* **2017**, *3*, eaap9252; b) Y. Wen, P. Zhang, V. K. Sharma, X. Ma, H.-C. Zhou, *Cell Rep. Phys. Sci.* **2021**, *2*, 100348; c) I. Ahmed, M. M. H. Mondol, H. J. Lee, S. H. Jhung, *Chem. Asian J.* **2021**, *16*, 185.

[7] a) S. Krause, N. Hosono, S. Kitagawa, *Angew. Chem., Int. Ed.* **2020**, *59*, 15325; b) A. Schneemann, V. Bon, I. Schwedler, I. Senkovska, S. Kaskel, R. A. Fischer, *Chem. Soc. Rev.* **2014**, *43*, 6062; c) P. Zhao, S. C. E. Tsang, D. Fairen-Jimenez, *Cell Rep. Phys. Sci.* **2021**, *2*, 100544; d) F. Bigdeli, C. T. Lollar, A. Morsali, H.-C. Zhou, *Angew. Chem., Int. Ed.* **2020**, *59*, 4652; e) S. Horike, S. Shimomura, S. Kitagawa, *Nat. Chem.* **2009**, *1*, 695.

[8] J. A. Mason, J. Oktawiec, M. K. Taylor, M. R. Hudson, J. Rodriguez, J. E. Bachman, M. I. Gonzalez, A. Cervellino, A. Guagliardi, C. M. Brown, P. L. Llewellyn, N. Masciocchi, J. R. Long, *Nature* **2015**, *527*, 357.

[9] a) R.-B. Lin, S. Xiang, H. Xing, W. Zhou, B. Chen, *Coord. Chem. Rev.* **2019**, *378*, 87; b) O. T. Qazvini, V.-J. Scott, L. Bondorf, M. Ducamp, M. Hirscher, F.-X. Coudert, S. G. Telfer, *Chem. Mater.* **2021**, *33*, 8886.

[10] J. Wieme, S. M. J. Rogge, P. G. Yot, L. Vanduyfhuys, S.-K. Lee, J.-S. Chang, M. Waroquier, G. Maurin, V. van Speybroeck, *J. Mater. Chem. A* **2019**, *7*, 22663.

[11] A. P. Katsoulidis, D. Antypov, G. F. S. Whitehead, E. J. Carrington, D. J. Adams, N. G. Berry, G. R. Darling, M. S. Dyer, M. J. Rosseinsky, *Nature* **2019**, *565*, 213.

[12] H. Kajiro, A. Kondo, K. Kaneko, H. Kanoh, *Int. J. Mol. Sci.* **2010**, *11*, 3803.

[13] a) G. Férey, *Chem. Soc. Rev.* **2008**, *37*, 191; b) F. Millange, R. I. Walton, *Isr. J. Chem.* **2018**, *58*, 1019; c) S. Vandenhaute, S. M. J. Rogge, V. van Speybroeck, *Front. Chem.* **2021**, *9*, 718920; d) T. Loiseau, C. Serre, C. Huguenard, G. Fink, F. Taulelle, M. Henry, T. Bataille, G. Férey, *Chemistry* **2004**, *10*, 1373.

[14] a) L. Vanduyfhuys, S. M. J. Rogge, J. Wieme, S. Vandenbrande, G. Maurin, M. Waroquier, V. van Speybroeck, *Nat. Commun.* **2018**, *9*, 204; b) F.-X. Coudert, *Chem. Mater.* **2015**, *27*, 1905; c) R. Demuynck, S. M. J. Rogge, L. Vanduyfhuys, J. Wieme, M. Waroquier, V. van Speybroeck, *J. Chem. Theory Comput.* **2017**, *13*, 5861.

[15] a) G. Fraux, F.-X. Coudert, *Chem. Commun.* **2017**, *53*, 7211; b) F.-X. Coudert, *Bull. Jpn. Soc. Coord. Chem.* **2019**, *73*, 15; c) V. van Speybroeck, S. Vandenhaute, A. E. J. Hoffman, S. M. J. Rogge, *Trends Chem.* **2021**, *3*, 605.
[16] a) S. Hiraide, Y. Sakanaka, H. Kajiro, S. Kawaguchi, M. T. Miyahara, H. Tanaka, *Nat. Commun.* **2020**, *11*, 3867; b) D. J. Cerasale, D. C. Ward, T. L. Easun, *Nat. Rev. Chem.* **2022**, *6*, 9.
[17] J. D. Evans, V. Bon, I. Senkovska, H.-C. Lee, S. Kaskel, *Nat. Commun.* **2020**, *11*, 2690.
[18] a) L. Schaper, J. Keupp, R. Schmid, *Front. Chem.* **2021**, *9*; b) J. Keupp, R. Schmid, *Adv. Theory Simul.* **2019**, *2*, 1900117.
[19] S. M. J. Rogge, M. Waroquier, V. van Speybroeck, *Nat. Commun.* **2019**, *10*, 4842.
[20] F. Salles, G. Maurin, C. Serre, P. L. Llewellyn, C. Knöfel, H. J. Choi, Y. Filinchuk, L. Oliviero, A. Vimont, J. R. Long, G. Férey, *J. Am. Chem. Soc.* **2010**, *132*, 13782.
[21] A. D. Lueking, C.-Y. Wang, S. Sircar, C. Malencia, H. Wang, J. Li, *Dalton Trans.* **2016**, *45*, 4242.
[22] N. Hosono, A. Terashima, S. Kusaka, R. Matsuda, S. Kitagawa, *Nat. Chem.* **2019**, *11*, 109.
[23] a) N. Klein, H. C. Hoffmann, A. Cadiau, J. Getzschmann, M. R. Lohe, S. Paasch, T. Heydenreich, K. Adil, I. Senkovska, E. Brunner, S. Kaskel, *J. Mater. Chem.* **2012**, *22*, 10303; b) V. Bon, N. Klein, I. Senkovska, A. Heerwig, J. Getzschmann, D. Wallacher, I. Zizak, M. Brzhezinskaya, U. Mueller, S. Kaskel, *Phys. Chem. Chem. Phys.* **2015**, *17*, 17471; c) N. Klein, C. Herzog, M. Sabo, I. Senkovska, J. Getzschmann, S. Paasch, M. R. Lohe, E. Brunner, S. Kaskel, *Phys. Chem. Chem. Phys.* **2010**, *12*, 11778; d) S. Ehrling, I. Senkovska, V. Bon, J. D. Evans, P. Petkov, Y. Krupskaya, V. Kataev, T. Wulf, A. Krylov, A. Vtyurin, S. Krylova, S. Adichtchev, E. Slyusareva, M. S. Weiss, B. Büchner, T. Heine, S. Kaskel, *J. Mater. Chem. A* **2019**, *7*, 21459.
[24] M. Sin, N. Kavoosi, M. Rauche, J. Pallmann, S. Paasch, I. Senkovska, S. Kaskel, E. Brunner, *Langmuir* **2019**, *35*, 3162.
[25] L. Abylgazina, I. Senkovska, S. Ehrling, V. Bon, P. St. Petkov, J. D. Evans, S. Krylova, A. Krylov, S. Kaskel, *CrystEngComm* **2021**, *23*, 538.
[26] S. Ehrling, M. Mendt, I. Senkovska, J. D. Evans, V. Bon, P. Petkov, C. Ehrling, F. Walenszus, A. Pöppl, S. Kaskel, *Chem. Mater.* **2020**, *32*, 5670.
[27] a) S. Watanabe, H. Sugiyama, H. Adachi, H. Tanaka, M. T. Miyahara, *J. Chem. Phys.* **2009**, *130*, 164707; b) F. Formalik, A. V. Neimark, J. Rogacka, L. Firlej, B. Kuchta, *J. Colloid Interface Sci.* **2020**, *578*, 77.
[28] L. Abylgazina, I. Senkovska, R. Engemann, S. Ehrling, T. E. Gorelik, N. Kavoosi, U. Kaiser, S. Kaskel, *Front. Chem.* **2021**, *9*, 674566.
[29] N. Kavoosi, V. Bon, I. Senkovska, S. Krause, C. Atzori, F. Bonino, J. Pallmann, S. Paasch, E. Brunner, S. Kaskel, *Dalton Trans.* **2017**, *46*, 4685.
[30] S. Ehrling, H. Miura, I. Senkovska, S. Kaskel, *Trends Chem.* **2021**, *3*, 291.
[31] a) T. J. W. De Bruijn, W. A. De Jong, P. J. Van Den Berg, *Thermochim. Acta* **1981**, *45*, 315; b) P. Krüger, *J. Phys. Chem. Solids* **1993**, *54*, 1549.